CHALMERS
UNIVERSITY OF TECHNOLOGY

Stress-corrosion cracking sensitization by hydrogen upon oxidation of nickel-base alloys by water – An experiment-guided first-principles study

Citation for the original published paper (version of record):
Meier de Andrade, A., Geers, C., Chen, J. et al (2024). Stress-corrosion cracking sensitization by hydrogen upon oxidation of nickel-base alloys by
water – An experiment-guided first-principles study. Journal of Nuclear Materials, 595.
http://dx.doi.org/10.1016/j.jnucmat.2024.155044

Journal of Nuclear Materials 595 (2024) 155044

Contents lists available at ScienceDirect

Journal of Nuclear Materials

journal homepage: www.elsevier.com/locate/jnucmat

Stress-corrosion cracking sensitization by hydrogen upon oxidation of nickel-base alloys by water – An experiment-guided first-principles study

Ageo Meier de Andrade [a,*], Christine Geers [a], Jiaxin Chen [a,b], Itai Panas [a]

[a] Department of Chemistry and Chemical Engineering, Chalmers University of Technology, Gothenburg, 41296, Sweden
[b] Studsvik Nuclear AB, Sweden

HIGHLIGHTS

- Nickel oxide hydration/dehydration reactions are understood to be a short-circuiting pathway for the inward diffusion of water to the alloy/oxide interface.
- Nickel oxy-hydroxide inclusions in the oxide scale serve oxidant towards chromia formation.
- Hydrogen catalyses a cyclic chromium oxidation process which maintains the growth of particulate nickel metal embedded in the oxide scale.
- The confinement of the alloy/oxide interface where chromium oxidation takes place implies that hydrogen evolution is hindered.
- Consequences of hydrogen pick-up are: (i) embrittlement of alloy grain boundaries; (ii) pinning of alloy vacancies, thus mitigating chromium mobility.

GRAPHICAL ABSTRACT

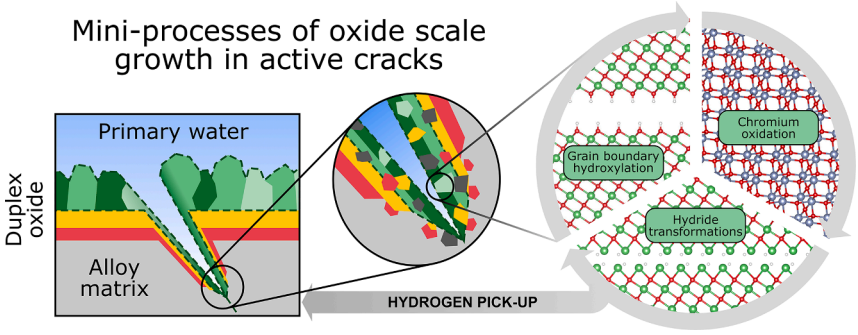

ARTICLE INFO

Keywords:
Density functional theory
Ni-base alloys
Hydrogen pick-up
Stress corrosion cracking
Sensitization

ABSTRACT

This work describes a viable hydrogen-induced sensitisation process toward stress corrosion cracking in chromia-forming nickel base alloys owing to oxidation by water. A mechanistic chemical understanding of the stress corrosion based on repeated cracking and re-healing of the oxide scale emerges from experiment-guided first-principles calculations. Piggybacking processes during repeated oxide scale cracking-healing cycles are understood to cause sensitisation towards the formation and growth of macroscopic cracks. Under light-water reactor conditions, the healed oxide scale comprises an outer region composed of chromium depleted nickel ferrite, and non-protective chromia, nickel oxide, and nickel hydroxide. An inner nickel iron chromite layer provides the passivating barrier that controls the oxidation rate at a steady state. Early during the re-healing of a crack in the oxide scale, water is conveyed to the alloy/scale interface by hydration/dehydration of composite nickel oxy-hydroxide $Ni(OH)_2$•NiO inclusions in the scale. At later stages, $Ni(OH)_2$•NiO serves as oxidant of preferentially chromium, while hydrogen is released as H_2(g) into the primary water or becomes picked up by the alloy, possibly while assisting in the reduction of NiO to form nickel metal particles. Oxidation by water equivalents at the confining alloy/oxide scale interface favours hydrogen pick-up in the alloy that becomes increasingly

* Corresponding author.
E-mail address: ageo@chalmers.se (A.M. de Andrade).

https://doi.org/10.1016/j.jnucmat.2024.155044
Received 27 November 2023; Received in revised form 29 February 2024; Accepted 19 March 2024
Available online 24 March 2024

detrimental owing to enrichment and inward diffusion of hydrogen along alloy grain boundaries. The pinning of alloy vacancies by hydrogen causes mitigation of outward diffusion of chromium, which in turn hampers crack re-healing while promoting alloy embrittlement.

1. Introduction

Structural alloys are exposed to load-induced stress fields that render them vulnerable to corrosion owing to the intermittent cracking of the passivating oxide scale. This stress corrosion that may lead to component failure, i.e., stress corrosion cracking (SCC), is a safety concern in pressurised water reactors (PWR) in nuclear power plants where these alloys mainly refer to chromia formers, such as the Ni-base alloys 600 and 690 [1,2]. For a failure in structural components due to SCC, it is necessary to have three aspects: a susceptible material or condition, stress, and environment [2]. No proven unified mechanism predicts or even explains how these factors affect crack susceptibility in actual plant conditions [3–5]. Still, various mechanisms have been proposed, but they only explain crack susceptibility under specific conditions involving one or a few factors related to SCC. These mechanisms can be classified into three large groups [6]: (i) oxidation/dissolution, including slip-step film rupture oxidation, internal oxidation, and enhanced surface mobility; (ii) hydrogen-assisted cracking (HAC) and hydrogen-induced cracking (HIC); (iii) mechanically oriented models, such as vacancy condensation and creep-assisted grain boundary rupture. In this work, we consider microscopic stress-corrosion/erosion of the oxide scale associated with intermittent local cracking and healing of the oxide scale as sensitisers towards hydrogen-promoted macroscopic cracking. We describe a pathway for water permeation by an inner cathode mechanism that contributes to the inward oxide scale growth. The driver for this mechanism is chromium oxidation by water, leading to sensitisation of alloy grain boundaries toward hydrogen-induced component failure.

Clearly, repeated healing of cracks will require a corresponding supply of chromium from the alloy into the cracked region. Kinetic concerns regarding chromium activity at the crack tip become decisive for the healing process [7,8]. This was observed in alloy 600 (15 at% Cr) and justified its replacement by alloy 690 (30 at% Cr) [9]. Consequently, the latter is used in many manufactured components of both PWR and BWR, such as steam generators and vessel head penetration nozzles [10,11]. Yet, in as much as healing is associated with the consumption of chromium, as of today, it is not clear whether alloy 690 becomes prone to cracking after a very long (approx. 40 years) operation or after extending its service life to 60 or even 90 years, as the life extension of LWR reactors is being currently discussed. This has justified laboratory studies that model potential long-term effects by mechanical accelerated ageing experiments [12,13]. Arguably, these approaches may have severe drawbacks, which make them unrealistic compared to operating conditions. Moreover, chemical and kinetic aspects to the aging process is missing in these experiments, as access to chromium, i.e., its activity, besides concentration in the alloy, relies on its mobility, which in turn is facilitated by atomic vacancies in the alloy matrix [13,14]. The mobility of vacancies, however, is understood to become increasingly mitigated by the uptake of atoms from the environment, critically including hydrogen [15–18].

At this stage, two different origins of hydrogen may affect corrosion processes in alloys under plant operation. One is the dosage of molecular hydrogen into the reactor water, which has been proven to attenuate crack propagation rates [19]. This, however, should not be confused with the hydrogen uptake into the alloy material, which takes place under non-equilibrium conditions, and attributed to hydrogen being released upon metal oxidation by water. Under equilibrium or steady-state conditions, the oxide scale reduction by hydrogen and its reoxidation by water, whereby hydrogen is being released, provides a channel to control oxide scale growth rates as well as composition. This near-equilibrium attenuation of the oxide scale by the hydrogen gas dosing in the coolant has implications for oxide scale thickness and morphology prior to cracking. Moreover, it affects the rate of the oxide scale healing following the intermittent stress-induced cracking and erosion of the oxide scale. Indeed, in experimental models of crack tips [20], the external H_2 dosage has been seen to influence hydrogen pick-up owing to the rapid oxidation by water. The hydrogen-induced embrittlement is owing to the fraction of hydrogen that is released and subsequently incorporated into the alloy microstructure during the metal oxidation process [21,22]. The viability of the latter, i.e., hydrogen pick-up owing to oxidation by water, is further substantiated in the present study.

Experimental results show that this second type of “free” hydrogen, once picked up by the alloy matrix, interacts with defects, thus decorating grain boundaries [23–25]. These decorated grain boundaries are susceptible to embrittlement and hydrogen-induced cracking [26], which may cause catastrophic failures of structural materials in a nuclear reactor. To assess whether hydrogen pick-up resulting from oxidation by water may become a decisive factor in SCC under nuclear power plant conditions, a viable mechanism for the uptake must be provided. The objective of the present study is to provide such a mechanism while at the same time considering the complex composition of the oxide scale in the vicinity of the crack tip.

Fig. 1 depicts two possible cracking scenarios associated with SCC. Here, it becomes useful to remind of what comprises the protective oxide scale of Ni-base chromia former alloys from various experimental works from the literature [14,27–37]. The protective scale is composed of an outer oxide layer shielding the resulting low pO_2 interior region near the alloy/oxide interface from the exterior oxidising environment [28–32]. Such a composite structure readily evolves in thermally grown oxides on nickel base alloys, albeit the composition of the outer scale transforms from iron and/or nickel chromite to predominantly nickel ferrite owing to solid-state transformations in the form of Cr-rich spinel, cf. Fig. 1.1 [28,33,34]. The low-pO_2 in vicinity of the alloy-oxide interface warrants a very thin chromia layer as chromium oxidises more readily than both iron and nickel at the interface between (Ni, Fe)Cr_2O_4 and the alloy matrix. The thin and compact chromia and chromite spinel are capped by the resulting outer protective nickel ferrite that is overgrown by non-protective residual of nickel oxide and nickel hydroxide, cf. Fig. 1.2. Instantaneous deep cracks suddenly expose the alloy interior and remnants of the chromia scale to the surrounding aqueous oxidising environment, rendering the latter prone to solid-state transformations [14]. Under benign conditions, the protective oxide scale is restored, i.e., cracks become stagnant, cf. Fig. 1.3a [14]. In these cases, the requirements for crack healing become satisfied, in that the initial irregular concurrent $NiO/Ni(OH)_2$, Fe_2O_3, and Cr_2O_3 formation, in the cracked region on slow-down allows formation of the passivating $NiFe_2O_4$ and (Ni,Fe)Cr_2O_4 spinels. Repeated cracking and healing are understood to render the stressed region depleted in chromium even though the overall composition of the alloy contains an excess of chromium [14]. This is because the Ni:Cr in the (Ni,Fe)Cr_2O_4 spinel is less than 1:2 while it is of the order 1:0.6 in alloy 690. Indeed, repeated cracking may render chromium activity at the crack tip insufficient for the protective oxide structure to form, cf. Fig. 1.3b [14,35]. Due to the exhaustive healing process, continuous crack propagation results in cases where protective oxide formation is hindered [35], either by a discontinuous outer scale or insufficient chromium activity to form the protective spinel.

In an active crack, the defective outer oxide scale is composed of the transient (Ni,Fe)Cr_2O_4 and the $NiFe_2O_4$ spinel, as well as NiO and

remnant Cr_2O_3 owing to the continuous chromium loss that comes in contact with the alloy matrix [28,33,34]. This complex oxide acts as an oxidant towards the alloy, whereby new chromia is formed. Thus, the resulting oxide reportedly includes also chromia and nickel metal as nickel oxide oxidises residual chromium at the crack tip [36,38,39]. Besides acting oxidising agent, NiO may react with coolant (water) to form $Ni(OH)_2$ which in turn may react with residual chromium in the alloy to form non-protective chromia, thus NiO can be understood to provide a short-circuiting path for chromium oxidation by water molecules. In doing so, H^+ from hydroxyl groups must be reduced to produce e.g., molecular hydrogen, hydrides in nickel particles or accommodation in oxygen vacancies in the vicinity of the crack tip, i.e., a nickel oxy-hydride interface, and/or by hydrogen pick-up in the alloy. Hydrogen pick-up is known to mitigate metal atom mobility in the alloy [16,25,40], here the outwards diffusion of chromium. This, in turn, effectively favours inward diffusion of water equivalents to oxidise the stagnant chromium that may result in grain-boundary embrittlement as well as guide crack propagation.

In the present study, first-principles calculations are utilised to identify viable pathways for hydrogen pick-up owing to the oxidation of chromium by water. The complex composition in the crack tip region, as determined in experimental studies, provides boundary conditions and evidence for chemical transformations presumably at the steady-state, e.g., $NiO/Ni(OH)_2$ and Cr_2O_3 reacting to form $NiCr_2O_4$. The resulting oxidation reaction is subdivided into mini-processes, each comprising of reactants, intermediates, and products. Thus, a viable mechanistic understanding of factors contributing to SCC and embrittlement is sought from the disentanglement of the complex chemical transformations at the crack tip region. This methodology has been successfully applied previously, e.g., chromic acid desorption from a Cr_2O_3 surface [41], high-temperature oxidation of chromium in O_2 and in $O_2 + 10\ \%H_2O$ at 600 and 700 °C [42], to unravel electrochemical reaction pathways for hydrogen pick-up in zircaloy [21,22,43] to the interplay between reactive elements, alumina and water in alumina-forming alloys [44–47], to describe oxidation-driven chloride diffusion in magnetite scale on low-alloyed steel [48], as well as to describe the role of zinc in mitigating cobalt-60 uptake in boiling water reactor (BWR) conditions [49]. Here, our comprehensive approach demonstrates how nickel oxide may act water conveyer by transforming into nickel hydroxide, thereby providing a short-circuiting pathway for oxidant to reach chromium at the alloy/oxide interface. The fates of hydrogen during chromia formation include hydrogen evolution, a nickel oxy-hydroxy-hydride interface formation, and hydrogen pick-up in the alloy. While the H_2 evolution is employed as a reference, this reaction channel is understood to be kinetically hindered owing to the confining immediate surrounding at the alloy/oxide interface.

2. Modelling considerations

Spin-polarised calculations were performed based on density functional theory [50,51] in the implementation with plane waves [52] and pseudopotentials using the CASTEP code [53] within the Materials Studio framework. The Perdew, Burke, and Ernzerhof (PBE) GGA functional [54,55] was employed in all calculations. Core electrons were described by on-the-fly generated norm-conserving pseudopotentials [56], and a plane-wave energy cut-off was set to 1200 eV. The *k*-point sampling of the Brillouin zone was made by means of the Monkhorst-Pack scheme [57,58] with a *k*-point separation of 0.05 $Å^{-1}$ for all structures. The electronic structure was minimised until the total energy difference was smaller than 10^{-7} eV/atom for two consecutive SCF cycles. A Gaussian smearing scheme with a width of 0.1 eV was used to facilitate convergency. All structures were fully optimised using the L-BFGS [59,60] algorithm with a total energy convergence tolerance of 10^{-5} eV/atom, maximum force tolerance of 0.03 eV/Å, maximum stress tolerance of 0.05 GPa, and maximum displacement tolerance of 10^{-3} Å.

The initial bulk structures for further geometry optimisations were obtained primarily from the Materials Studio database and the inorganic crystal structure database (ICSD) [61]. Optimised structures were then compared with experimental lattices reported in ICSD, and the percentage error was calculated. Table 1 summarises the bulk structures,

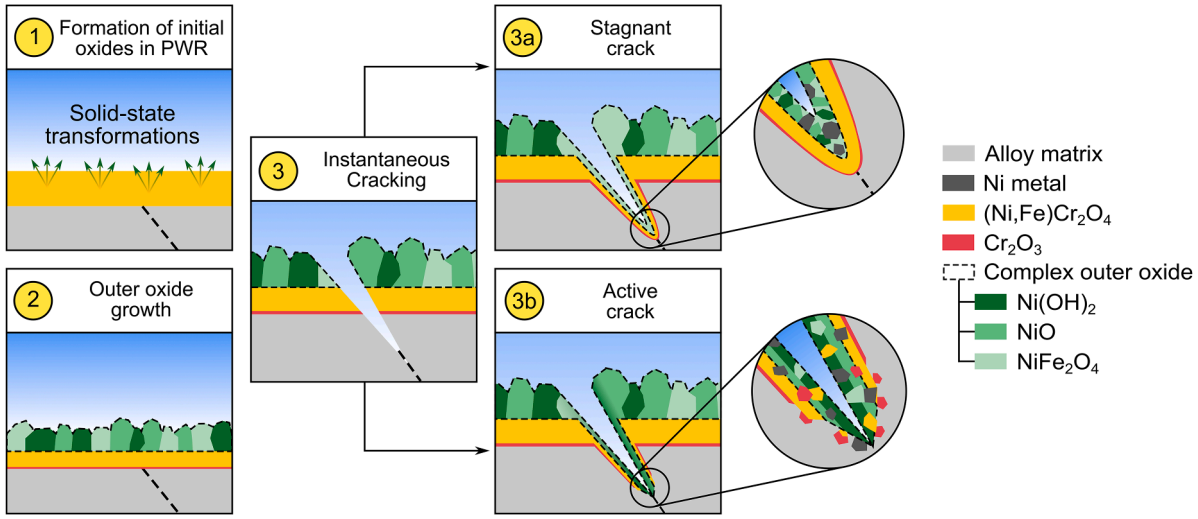

Fig. 1. Schematic representation of oxide growth and two types of intergranular cracks observed in Ni-base alloys. (1) The initial oxide that is formed when in contact with primary water in a PWR environment is a mixed $(Ni,Fe)Cr_2O_4$ (yellow). (2) The outer oxide scale results from solid-state reactions of $(Ni,Fe)Cr_2O_4$, which transforms the original oxide scale into a complex oxide composed of $Ni(OH)_2$, NiO, and $NiFe_2O_4$, represented by the various shades of green in the dashed region. The complex outer oxide protects the $(Ni,Fe)Cr_2O_4$ scale from chromium dissolution/reprecipitation, allowing for a very thin and compact Cr_2O_3 scale (red) at the interface with the alloy matrix. (3) Stress corrosion of the complex oxide scale exposes the alloy matrix to the primary water, causing further oxidation of grain boundaries (black dashed line in the alloy matrix) in the cracked region. (3a) Under benign conditions, the chromium activity is sufficient to form a very thin, well-adherent compact chromia scale surrounding the crack which, in conjunction with the initial and outer oxide scales, impedes propagation along the alloy grain boundaries, i.e., the crack is stagnant. (3b) When the chromium activity near the oxide cracked region is insufficient, the mixed complex oxides formed at the crack tip cannot protect against propagation. Thus, the open crack allows further oxidation of the alloy by primary water that is mainly conveyed by hydroxylated/oxidised grain boundaries.

Table 1
Cell parameters for the bulk systems. Values in parenthesis correspond to the calculated percentage error with respect to the experimental values from the reference data in the table.

	Unit cell parameters (Å)					
	Experiment			This work, GGA-PBE (%err)		
System	a	b	c	a	b	c
Fe_2O_3 (hematite)[a]	5.035	5.035	13.747	5.029 (−0.111)	5.029 (−0.111)	13.921 (1.270)
Fe_3O_4 (magnetite)[b]	5.935	5.935	5.935	5.956 (0.365)	5.956 (0.365)	5.956 (0.365)
NiO[c]	4.178	4.178	4.178	4.196 (0.436)	4.196 (0.436)	4.196 (0.436)
$Ni(OH)_2$ [d,e]	3.126	3.126	4.605	3.248 (3.900)	3.249 (3.934)	4.501 (−2.254)
Ni[f]	3.524	3.524	3.524	3.562 (−1.087)	3.562 (−1.087)	3.562 (−1.087)
Cr_2O_3 [g]	4.957	4.957	13.592	4.939 (−0.348)	4.939 (−0.348)	13.847 (1.883)
$NiCr_2O_4$ [h]	8.309	8.309	8.309	8.354 (0.537)	8.354 (0.537)	8.354 (0.537)

a) Experimental data from [62].
b) Experimental data from [63].
c) Experimental data from [64].
d) Experimental data from [65].
e) Calculated lattice parameters with applied external pressure of 1 GPa along the c axis, see text.
f) Experimental data from [66].
g) Experimental data from [67].
h) Experimental data from [68].

experimental and calculated lattice parameters and %err.

The kinship between $NiO+Cr_2O_3$ oxide mix and $NiCr_2O_4$ may be understood from the negligible difference in enthalpies of formation, i.e.,

$$NiO + Cr_2O_3 \rightarrow NiCr_2O_4$$

Based on our DFT calculations we obtain $\Delta H_{DFT} = -6.74$ kJ/mol for the above reaction, in close agreement with the experimentally reported $\Delta H_{exp} = -5.31$ kJ/mol [69], which is only a marginal energy gain with respect to chromium oxidation by NiO. Furthermore, the fact that formation of $NiCr_2O_4$ is kinetically controlled tells of rapid early formation of $Ni(OH)_2$ / Cr_2O_3 mix which later reacts to passivating $NiCr_2O_4$ [28].

2.1. Nickel oxide lamellae interface models

The interface supercells were obtained starting from the brucite structure of β-$Ni(OH)_2$. It comprises a stack of monolayers of edge sharing oxygen octahedra forming a coordination cage around Ni(II) ions, the top and bottom oxygen ions are protonated. An external pressure was applied along the stacking c-direction. This was done partly to compensate for the lack of dispersion interactions within the GGA-DFT formalism and partly to mimic the build-up of lateral stresses upon oxide scale growth. Taking the external pressure as a free parameter, the computed interlayer distances of β-$Ni(OH)_2$ for pressures in the range 0 to 4.5 GPa were fitted to approximate experiment. An external pressure of 1 GPa was thus obtained, see Table 1. An additional 1 GPa was employed in all subsequent interface calculations as it mimics the build-up of lateral stress during oxide scale growth. Indeed, 2 GPa is within the range of what is experimentally observed [70–72].

The nickel oxy-hydroxide interfaces are understood to comprise lamellae composed of NiO cores and hydroxylated interfaces. Such interface naturally evolves by the release of water upon subjecting the stacked monolayers in β-$Ni(OH)_2$ to condensation reactions. The nickel oxy-hydroxide interface also has structural compatibility between the NiO rocksalt surface structure along the (111) growth direction and the layered β-$Ni(OH)_2$ structure along the (001) stacking direction, c.f. Fig. 2 top view. For all interfaces, the oxy-hydroxide lamella thickness is defined by the number of Ni atoms x in the supercell, where one Ni atom defines a thickness unity. Lamellae of $x = 4$, 6 and 8 layers were considered in this work.

The chromium oxidation reaction with the nickel oxy-hydroxide interface produces nickel oxy-hydrides. The latter was built from the

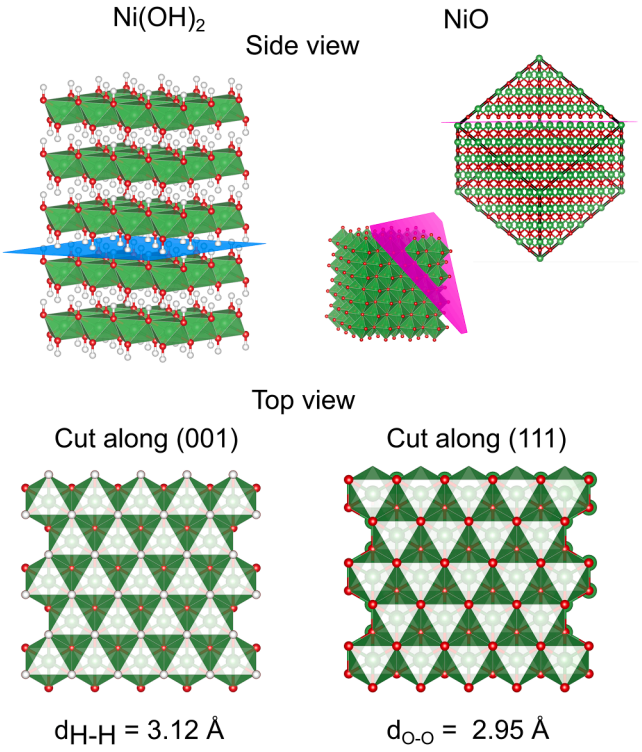

Fig. 2. Schematic representation of the coherence between the β-$Ni(OH)_2$ (001) – blue plane – and NiO(111) – pink plane – surfaces. The bulk structures and their respective coherent lattice planes are shown in the top panel. For the rocksalt NiO, two side views are shown, where the topmost view evidence that the cut along the (111) direction separates Ni and O bonds that are further hydroxylated in an aqueous environment, creating two equivalent OH-terminated NiO(111) surfaces. The left figure on the lower panel shows a top view of the cut along the (001) plane of β-$Ni(OH)_2$, and the right figure shows a cut along the (111) plane of NiO. To further evidence the coherence between the β-$Ni(OH)_2$ (001) and the oxygen-terminated NiO(111) surfaces, the experimental lateral distance between hydrogen atoms in the former and oxygen atoms in the latter are listed [64,73].

optimised nickel oxy-hydroxide by removing the oxygen from the hydroxyl groups and moving the hydrogen to the oxygen vacancy positions. Finally, to obtain the enthalpy of reaction involving hydrogen pick-up, the nickel oxy-metal interface was built from the nickel oxy-hydride by removing all hydrogen atoms of the supercell.

3. Results and discussion

3.1. Hydroxylation of nickel oxide particles by primary water

Upon instantaneous cracking, see Fig. 1.3b, remnants of the fractured oxide as well as the alloy matrix are exposed to the high-temperature coolant. The initial and subsequent oxidation of the crack tip produces an irregular and poorly passivating "junk oxide" composite that is chromia and iron oxides, nickel oxide, and nickel hydroxide. The latter has two polymorphs: α-$Ni(OH)_2$ with intercalated water molecules that crystallise into the brucite β-$Ni(OH)_2$ polymorph [74].

The transformation of α-$Ni(OH)_2$ into β-$Ni(OH)_2$ occurs as loosely bound molecular water, intercalated between Ni(II) layers, vaporises upon heating. Moreover, it is concluded from thermogravimetry (TG) analysis of β-$Ni(OH)_2$ that vaporisation exclusively involving intercalated water molecules takes place at a temperature of around 160 °C [75]. This is followed by a broad TG feature between 170 and 525 °C, where the condensation reactions that transform β-$Ni(OH)_2$ into NiO + H_2O and the water evaporation occur simultaneously and in parallel [76]. This supports the notion that under PWR (BWR) operating temperatures i.e., 320 °C (275 °C), various composites of $Ni(OH)_2$ and NiO in the oxide scale may indeed further participate in the chromium oxidation reaction by conveying water from the coolant to the crack tip.

Condensation of the layered β-$Ni(OH)_2$ produces an intercalation compound of nickel oxide where lamellae grow along the (111) direction while exhibiting the hydroxide termination; see Fig. 3 schematically showing two possible reactions involving water to produce the oxy-hydroxide interface. At this stage, the effective oxidation potential is reflected in the activity of the short-circuiting $Ni(OH)_2{\cdot}(NiO)_{x-1}$ – nickel oxy-hydroxide – fraction of the scale. Such topotactic structure is produced when nickel oxide is hydrolysed and forms nickel hydroxide incorporated in nickel oxide at the coolant/oxide interface or by a condensation reaction of nickel hydroxide that is converted back to nickel oxide at the oxide/alloy interface, as illustrated in Fig. 3. Microscopic studies of active crack tips of Ni-base alloys are consistent with this understanding [28,29,35,77–80].

The interface region of the $Ni(OH)_2{\cdot}(NiO)_{x-1}$ intercalation compound may be subjected to chemical transformations. The water conveying mechanism along the lamella proposed in this work is thus understood to compete with the lamella fusing condensation processes. This results in water, as mediated by nickel oxide, effectively oxidising chromium. Correspondingly, the nickel oxide hydration/dehydration processes effectively transfer the cathode to the oxide/alloy interface by protons and hydroxide co-diffusion along oxide grain boundaries, thereby determining the rate of oxidation. The increased fraction of $Ni(OH)_2{\cdot}(NiO)_{x-1}$ in the cracked region in the oxide scale, owing to the irregular oxidation processes at early stage of crack healing, lends increased importance to the inner cathode mechanism, which is supported by the inward diffusion of electro-neutral water equivalents, i.e., protons and hydroxide ions, from the coolant/oxide interface to the oxide/alloy interface.

Validation of the proposed mechanism of nickel oxide effectively mediating water to the alloy/oxide interface includes evaluating the stability of the partially condensed [-hydroxide|oxide|hydroxide–hydroxide|oxide|hydroxide-] lamella structure. Here, we evaluate the energetics of the nickel oxy-hydroxide interface for different thicknesses of the oxide region. To benefit from error cancellation in periodic solid-state DFT calculations, bulk nickel hydroxide and nickel oxide are used as references, while the energetics for the reaction

$$NiO(s) + H_2O(l) \rightarrow Ni(OH)_2(s) \quad \text{(R1)}$$

is −13 kJ/mol and was taken from the experimental standard enthalpy of formation [81]. Thus, the stability of the lamella structure is arrived at by considering the solid-state reaction

$$Ni(OH)_2(s) + (x-1)NiO(s) \rightarrow Ni(OH)_2{\cdot}(NiO)_{x-1}(s) \quad \text{(R2)}$$

where $(x-1) = 3,\ 5,\ 7$ represents the number of NiO(s) layers in the

Table 2
Enthalpy of formation per one mol of H_2O molecule of the nickel oxy-hydroxide interface with three different thicknesses. These results refer to the energetics of the chemical reaction R2 calculated with GGA-PBE DFT. Note that the lamella thickness is defined as the number of nickel atomic layers in $Ni(OH)_2{\cdot}(NiO)_{x-1}$.

Number of Ni layers (lamella thickness)	ΔH_{DFT} (kJ/mol of H_2O molecules)
4	−33.64
6	−30.82
8	−31.45

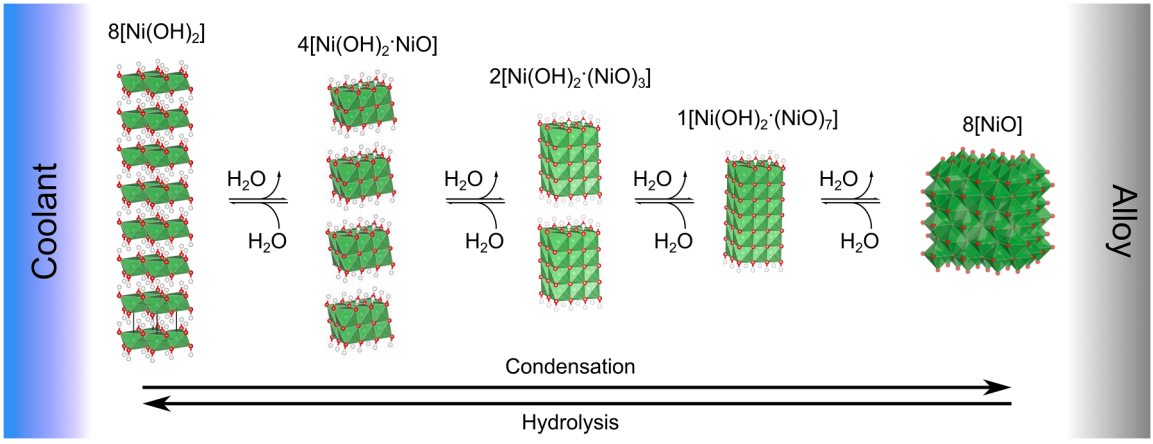

Fig. 3. Schematic representation of the condensation of nickel hydroxide (β-$Ni(OH)_2$, left) and the hydrolysis of nickel oxide (rocksalt NiO, right) in an aqueous environment in nuclear power plants. At the coolant-oxide interface, the condensation reaction starts with the recrystallisation of the α-$Ni(OH)_2$ (not shown) by releasing water to produce the fully hydroxylated brucite β-$Ni(OH)_2$, see the left-most structure, which may act as oxidant towards chromia formation. The consequence is the removal of stochiometric water equivalents ($OH^- + H^+$) from the hydroxylated interface (representing hydroxylated grain boundaries) to produce thicker oxy-hydroxide lamella. As water is consumed in the chromium oxidation reaction, hydroxylated grain boundaries are lost, thus fusing interfaces and producing NiO particles (right).

intercalation compound, the structure of which is obtained by hydrolysis along (111) planes, schematically represented in Fig. 3. The results of the hydrolysis are shown in Table 2. The isodesmic nature of the reaction warrants that the reaction energy obtained by DFT is a good approximation of the enthalpy of reaction ΔH_{DFT}.

The results presented in Table 2 show that the hydroxylation of oxygen-terminated NiO(111) surface interfaces are favourable (exothermic) by approximately 30 kJ/mol, regardless of the NiO lamella thickness. The significance of this result is further accentuated by the fact that the enthalpy of NiO hydration to form $Ni(OH)_2$ is exothermic by ~13 kJ/mol. Clearly, in cases where the availability of water limits the hydration of NiO(s), it becomes favourable to maintain NiO in the form of hydroxylated lamella compared to the case of a fully hydroxylated lamella, i.e., β-$Ni(OH)_2$. This robustness of the hydroxylated lamella supports the notion of their possible water-conveying role, i.e., hydration/dehydration serving a viable steady-state short-circuiting pathway across the oxide scale and thereby effectively allowing the oxidation of chromium by water to take place at the oxide/alloy interface. This result is in accordance with various work in the literature that report a favourable hydroxylation of oxygen-terminated NiO(111) surfaces [82–85].

In as much as water acts oxidant towards chromia formation, and the anode process taking place at the oxide/alloy interface, the complementary cathode process comprises the reduction of H^+. The significance of the water permeation channel by the oxy-hydroxide interface is to bring the cathode process closer to the anode at the metal-oxide interface, as compared to the hydrogen evolution reaction at the coolant/oxide interface. Thus, the semiconducting property of the early passivating oxide scale and complementary inward diffusion of oxygen ions and/or outward diffusion of cations is complemented by a short-circuiting effective inward diffusion of molecular water in the form of hydroxylated nickel oxide interfaces. One can say that there is a coexistence of two cathode processes, inner (hydrogen pick-up) and outer (hydrogen evolution), the latter slowing down with increased oxide thickness as the driving electrochemical potential gradient across the oxide scale diminishes, lends the short-circuiting inner cathode increased relative importance with time, i.e., hydrogen uptake by the alloy increases over time. Also, the further oxidation at late stages cooperates with oxide grains coarsening, and correspondingly, the number density of short-circuiting water carrying grain boundaries diminishes.

$$[OH^-]Ni(\mathrm{II})[OH^-]\cdot(NiO)_{x-1} + 4Fe_3O_4 \rightarrow [H^-]Ni(\mathrm{II})[H^-]\cdot(NiO)_{x-1} + 6Fe_2O_3 \quad \text{(R5)}$$

It is this ideal grain boundary density controlled sub-parabolic ($t^{1/3}$) scale growth kinetics which fails upon stress corrosion cracking.

3.2. Oxy-hydroxide interface as the oxidising agent in chromia formation

During passivation of a freshly cracked oxide scale on chromia forming Ni-based alloys, the rapidly formed initial scale is prone to chromium loss. In alloy 690, a fraction of Cr(III) in $(Ni,Fe)Cr_2O_4$ may undergo redistribution in the oxide scale. This, owing to the oxidising environment of water undergoing radiolysis whereby intermediate surface Cr(VI) species are formed and in turn undergo hydrolysis and dissolution as CrO_4^{2-}(aq) and subsequent reprecipitation. More importantly, the rapidly incoherently growing oxide scale supports the segregation of Cr_2O_3 to the extent that the remaining scale constitutes the nominal $NiFe_2O_4$ and NiO. Stabilities of $Ni(OH)_2\cdot(NiO)_{x-1}$ interfaces with varying thicknesses were provided in the previous section. The relevance of this observation is supported further by the experimentally reported 170–525°C temperature range for the transformation of β-$Ni(OH)_2$ to NiO on evolving H_2O(g) [74]. Thus, access at early stages to the inner cathode is provided by conveying molecular water along the said hydroxylated interface, an electrochemically driven process as the oxidation of the alloy by water results on condition of the complementary hydrogen evolution (outer cathode) reaction. At later stages, it becomes conceivable that the chromium oxidation diminishes hydroxylated interfaces, which in turn mitigates their rehydration in favour of NiO lamella coarsening [28,79,86].

For the sake of clarity and to evidence the role of hydrogen, H^+, and H^- in the chemical transformations discussed here, the nickel oxy-hydroxide interface will be described as $[OH^-]Ni(\mathrm{II})[OH^-]\cdot NiO$ in the chemical reactions from now on.

As oxygen from the hydroxide ion OH^- reacts with chromium metal, proton H^+ reduces to hydride H^- and populates the oxygen vacancy left at the interface, transforming the nickel oxy-hydroxide into an oxy-hydride interface, i.e.,

$$[OH^-]Ni(\mathrm{II})[OH^-]\cdot(NiO)_{x-1} + 4/3Cr(s) \rightarrow [H^-]Ni(\mathrm{II})[H^-]\cdot(NiO)_{x-1} + 2/3Cr_2O_3 \quad \text{(R3)}$$

Computing ΔH_{DFT} for this reaction is not as straightforward as for the stability of the oxy-hydroxide interface because the reaction is not isodesmic as the bonding characteristics change, i.e., chromium metal bonds convert to that in the oxide and hence disallowing the benefit of error cancellation. To correct for this, we calculate ΔH_{DFT} for reaction R3 by combining two chemical reactions:

1. reaction R4 below is the oxidation of chromium having hematite (Fe_2O_3) as the oxidising agent, thus forming chromium oxide and magnetite (Fe_3O_4), i.e.,

$$2/3Cr(s) + 3Fe_2O_3 \rightarrow 1/3Cr_2O_3 + 2Fe_3O_4 \quad \text{(R4)}$$

The enthalpy of formation for this reaction is taken from experiment: $\Delta H_{exp} = -144.09\ kJ/mol$ [81]. To ensure error cancellation, we use ΔH_{exp} instead of ΔH_{DFT}.

2. the second reaction R5 is the oxidation of magnetite by the oxy-hydroxide interface and restoring hematite, i.e.,

This way, the reaction enthalpy for the sought transformation is determined by combining ΔH_{DFT} and ΔH_{exp}, since the transformation of the oxy-hydroxide into the transient oxy-hydride (R5) is not experimentally available. From calculated ΔH_{DFT} for R5, it may be concluded that formation of the $[OH^-]Ni(\mathrm{II})[OH^-]$ moiety by oxidising magnetite to hematite becomes increasingly unfavourable with increased lamella

Table 3
Reaction enthalpy of magnetite oxidation by the oxy-hydroxide interface normalised by the number of hydrogen atoms for three different lamella thicknesses. These results refer to the energetics of the chemical reaction R5 calculated with GGA-PBE DFT.

Number of layers	ΔH_{DFT} (kJ/mol) per H atom
4	+32.13
6	+41.01
8	+73.69

Table 4
Reaction enthalpy of chromium oxidation by the oxy-hydroxide interface normalised by the number of hydrogen atoms for three different lamella thicknesses. These results refer to the energetics of the chemical reaction R3 calculated by combining ΔH_{exp} for R4 and ΔH_{DFT} for R5.

Number of layers	ΔH_{DFT} (kJ/mol) per H atom
4	−111.96
6	−103.07
8	−70.39

thickness, see Table 3. Offsetting the oxidation reaction R5 by ΔH_{exp} for R4 significantly drives for oxidation of the $[OH^-]Ni(II)[OH^-]$ lamellae, see Table 4.

It may be concluded that hydroxylated nickel oxide grain boundaries constitute viable oxidising agents toward chromia formation, whereby the protons transform into hydride ions and become accommodated in oxygen vacancies. This finding reinterprets the notion of non-protective porous NiO at the crack tip [38] as it adds the role of $Ni(OH)_2{\cdot}(NiO)_{x-1}$ as a water conveyer. This is to the extent that the hydroxylated interfaces eventually become consumed by the Cr oxidation process.

Ni-base alloys are known to not form stable hydride phases. However, a local hydride was experimentally observed immediately after hydrogen charging of a specimen composed of an alloy with approximately 22 wt% of chromium, but the authors showed that it decomposes after ageing at room temperature [87]. On the other hand, local hydrides are likely to form at the crack tip, e.g., by the nucleation of nickel oxy-hydrides, as described here. These may indeed constitute transients supporting the crack propagation in Ni-base alloys [86]. As much as hydride formation is known to support hydrogen embrittlement in load-bearing components, it is likely to impact SCC and crack propagation in Ni-base alloys [88].

3.3. The fate of hydrogen

The nickel oxy-hydroxy-hydride transients, that form as the nickel oxy-hydroxide oxidises chromium, may react further along three main paths. All three involve the formation of nominal Ni(0), i.e., Ni metal particles incorporated in the oxide scale. *In a first pathway,* H^+ and H^- may recombine to form H_2, that is the hydrogen evolution (outer cathode) channel. *For the second pathway,* H^+ and H^- may react with NiO to form $Ni(OH)_2$ that in turn oxidises Cr and recovers the $H^+ + H^-$ pair in a cyclic manner, rendering feasible the formation of metallic nickel particles in the oxide scale, as one Ni(0) is produced in each of such cycle. In fact, there has been a debate on the literature regarding the presence of pure Ni metal particles in oxidised grain boundaries of Ni-base alloys in PWR. Some authors claim that Ni metal is a result of sputtering during experiments [89], while others support the notion that unoxidised Ni metal from the alloy matrix is incorporated in oxide particles at grain boundaries [39,90]. The possibility we put forward here is that metallic Ni particles form a result of cyclic $H^+ + H^-$ assisted chemical transformations of NiO into Ni(0) inside the oxide scale, albeit in vicinity of the oxide/alloy interface. Lastly, *in a third pathway,* H^+ and H^- may be picked up by the alloy.

It is noted that in case of *first* and *third* channels one Ni(0) is formed per $H^+ + H^-$ pair, while the *second* cyclic channel represents a catalytic process for the thermodynamically preferred oxidation of 2/3Cr(0) by NiO to form $1/3Cr_2O_3$ and Ni(0). Each of the three reaction channels are addressed in the following.

Table 5
Reaction enthalpy for the hydrogen evolution reaction (HER) associated with the transformation of the nickel oxy-hydride into nickel oxy-metal interface. ΔH_{DFT} of the chemical reaction R6 is normalised by the number of hydrogen atoms for three different lamella thicknesses.

Number of layers	ΔH_{DFT} (kJ/mol)
4	+31.61
6	+32.04
8	+19.12

3.3.1. Hydrogen evolution reaction (HER) to form Ni(0)

On oxidation by water, H_2O effectively reacts with M(0) to form H_2 and MO where it is common to assign M to the role as anode, the reduction of H^+ being the cathode. In the present study, we explore the ability of NiO to effectively convey water, in the form of hydroxylated nickel oxide particles in grain boundaries, to the scale/alloy interface. An intermediate nickel oxy-hydroxy-hydride is formed because of the chromia formation, i.e., H^+ associated with hydroxide ions [O(-II)H(+I)]$^-$ become reduced to H^- upon chromia formation (see reaction R3). In this context, the hydrogen evolution reaction (HER) channel proceeds by recombining H^- and H^+ from the $[H^-]Ni(II)[H^-]$ moiety. Upon hydrogen evolution, the remaining electrons from the hydride moiety act as the reducing agent to form H_2, thus transforming Ni(II) into its metallic form Ni(0), i.e.,

$$[H^-]Ni(II)[H^-]{\cdot}(NiO)_{x-1} \rightarrow Ni(0){\cdot}(NiO)_{x-1} + H_2(g) \quad \text{(R6)}$$

It becomes interesting to find that this reaction is somewhat endothermic by 20–30 kJ/mol, see Table 5. What would make the reaction R6 spontaneous is the entropy associated with the release of the H_2 into the gas phase. Here, however, the confining surroundings near the scale/alloy interface would render the HER kinetically hindered as its realisation is conditioned by H_2 diffusion through the oxide scale grain boundaries [77]. This opens for other fates of hydrogen in the transient nickel oxy-hydroxy-hydride, than *a priori* HER, i.e., hydrogen being picked up by the alloy.

3.3.2. Hydrogen catalysed cyclic Ni(0) build-up in NiO

On liberating Ni(0), H^+ and H^- may react with NiO to form new $Ni(OH)_2$, i.e.,

$$[\boldsymbol{H}^-]Ni(II)[O\boldsymbol{H}^-]Ni(II){\cdot}(NiO)_n \rightarrow Ni(0){\cdot}[O\boldsymbol{H}^-]Ni(II)[O\boldsymbol{H}^-]Ni(II){\cdot}(NiO)_{n-1} \quad \text{(R7)}$$

Repeatedly, the $Ni(OH)_2$ in turn may act to oxidize Cr(0), while recycling hydrogen,

$$Ni(0)_m{\cdot}[\boldsymbol{H}^-]Ni(II)[O\boldsymbol{H}^-]Ni(II){\cdot}(NiO)_{n-m} \rightarrow Ni(0)_{m+1}{\cdot}[O\boldsymbol{H}^-]Ni(II)[O\boldsymbol{H}^-]Ni(II){\cdot}(NiO)_{n-m-1} \quad \text{(R8)}$$

Table 6
Reaction enthalpy for the cyclic Ni(0) build-up associated with the transformation of the nickel oxy-hydride into nickel oxy-hydroxide. ΔH_{DFT} is normalised by the number of hydrogen atoms for three different lamella thicknesses.

Number of layers	ΔH_{DFT} (kJ/mol) per H atom
4	−26.20
6	−24.98
8	−40.77

Table 7
Reaction enthalpy for hydrogen-vacancy complexes associated with the transformation of the nickel oxy-hydride into nickel oxy-metal interface. ΔH_{DFT} of the chemical reaction R9 is normalised by the number of hydrogen atoms for three different lamella thicknesses.

Number of layers	Hydrogen in the octahedral site adjacent to a vacancy ΔH_{DFT} (kJ/mol) per H atom	Hydrogen in the tetrahedral site adjacent to a vacancy ΔH_{DFT} (kJ/mol) per H atom
4	+7.30	+10.81
6	+7.72	+11.23
8	−5.20	−1.69

The corresponding enthalpies of formation are shown in Table 6. Our results show that a cyclic process is indeed thermodynamically favourable. Experimentally, Marchetti et al. reported the presence of nickel hydroxide for all corrosion durations of alloy 690 [29]. Also, Ni(0) is found in contact with NiO and Cr_2O_3 in grain boundaries [35,91,92]. The cyclic hydrogen catalysed process in vicinity of the scale/alloy interface that effectively facilitates the oxidation of Cr(0) by NiO to form Ni(0) and chromia may be sustained if the hydrogen activity is maintained there. Loss of hydrogen, i.e., H^+ and H^-, may happen owing to the HER or by hydrogen pick-up in the alloy. In the next session, we will describe a third possible chemical transformations that may happen at grain boundaries.

3.3.3. Hydrogen uptake

The third fate of hydrogen, besides the hydrogen evolution reaction and the catalytic hydrogen assisted oxidation of Cr(0) by NiO to form chromia and Ni(0), is hydrogen uptake by the alloy or in the growing Ni (0) particles incorporated in the oxide scale. While the solubility of hydrogen in Ni(0) is low, hydrogen pick-up and mobility in stainless steel and nickel base alloys is greatly enhanced when associated with metal atom vacancies. In as much as defects migrate to alloy grain boundaries, the GB:s are expected to become enriched by the so-called hydrogen-vacancy complexes, a topic has been extensively reported [21,93–95]. Here, we put this information into the context of corrosion of nickel-base alloys owing to hydrogen pick-up. For the results shown in Table 7, we consider the reaction enthalpy for hydrogen – that is ½(H^- + H^+) from nickel oxy-hydroxy-hydrides – being transferred into tetrahedral or octahedral sites adjacent to Ni vacancies in face-centred cubic Ni(s), i.e.,

$$\frac{1}{2}Ni(0)_m{\cdot}[H^-]Ni(II)[OH^-]Ni(II) + \left[V_{FCC-Ni(s)}\right] \rightarrow \frac{1}{2}Ni(0)_{m+1}{\cdot}NiO{\cdot}NiO + \left[V_{FCC-Ni(s)}^{H(adjacent)}\right] \quad \text{(R9)}$$

While it is tempting to conclude that the affinity of hydrogen to the FCC Ni(s) vacancies depends on the thickness of the resulting $Ni(0){\cdot}NiO$ lamellae, the fact that the enthalpy changes are small lend greater importance to any entropy changes associated with the hydrogen incorporation. This, considering the $T\Delta S$ contribution to the Gibbs free energy at the $T \approx 600$ K which is the operating temperature of PWRs. The competitiveness of the hydrogen pick-up channel is further strengthened considering the suppression of the hydrogen evolution reaction owing to the confining surroundings at the scale/alloy interface. Also, hydrogen pick-up is understood to terminate the highly correlated cyclic hydrogen catalysed NiO reduction by Cr(0) oxidation.

Table 8
Reaction enthalpy for the segregation of nickel oxy-metal interface into pure Ni(0) and NiO.

Number of layers	ΔH_{DFT} (kJ/mol)
4	−84.87
6	−105.09
8	−138.86

3.4. On granular Ni(0) in the oxide scale

The hydrogen-assisted oxidation of Cr(0) by NiO to form chromia and Ni(0) offers a mechanism for the formation of granular Ni(0) in the mixed oxide matrix. Connection with metal-oxide segregations as evidenced by microscopy studies [35,91,92] is made here by demonstrating the spontaneous further decomposition of the $Ni(0){\cdot}(NiO)_{x-1}$ lamellae, i.e.,

$$Ni(0){\cdot}NiO \rightarrow Ni(s) + NiO(s) \quad \text{(R10)}$$

The results are shown in Table 8. Thus, the Ni(0) terminated NiO lamellae – resulting from (R3) Cr(0) oxidation driven by nickel hydroxide $Ni(OH)_2$ condensation to model formation of hydroxide terminated nickel oxide grains; reduction of the said into nickel oxy-hydroxy-hydride moieties that are furthermore prone to either hydrogen evolution (R6) or hydrogen pick-up (R9), possibly following stages of hydrogen catalysed cyclic reduction of NiO to Ni(0) by further Cr(0) oxidation (R7 and R8) – are found to readily segregate into NiO and Ni (0).

3.5. Implications of the proposed mechanism for hydrogen pick-up owing to oxidation by water

The potential usefulness of the emerging understanding of stress corrosion cracking in terms of stress-induced intermittent microscopic cracking and re-healing of an *a priori* protective oxide scale, which in turn supports sensitisation processes towards macroscopic cracking and component failure, is highlighted. Here, it is owing to hydrogen pick-up, a secondary process that results from water acting oxidant. The chromium activity loss at the oxide scale interface is owing to hydrogen associating with vacancies in the alloy, preferentially along alloy grain boundaries. Thus, it mitigates the outward diffusion of Cr and supports the inward diffusion of oxygen into alloy grain boundaries.

The interplay between *physical* hydrogen added to the coolant to control the reducing potential and *chemical* hydrogen associated with molecular water has been experimentally observed previously [19,20]. Here, this is explained by *physical* hydrogen controlling the oxide scale thickness while also affecting the rate of re-healing. Thus, the *chemical* hydrogen pick-up during scale cracking and re-healing is little affected at low partial pressures of molecular hydrogen. On increasing the pH_2, the chemical oxidation reaction still causes fractional hydrogen pick-up, while the parallel reduction reaction described in this work renders the scale re-healing process slowed down. At high pH_2, the thin oxide scale is less sensitive to mechanical stresses and thus the stress corrosion is much suppressed. A "sweet spot" that maximises the hydrogen pick-up at a particular pH_2 is inferred in agreement with the experimental observations [19,20].

4. Conclusions

This work reports a comprehensive understanding of crack tip oxidation in chromia-forming nickel base alloys relevant to the sensitisation of alloy grain boundaries towards stress corrosion cracking. As the oxidising agent, water is effectively conveyed to the oxide/alloy interface to react with chromium to form chromia. The build-up of a new protective oxide scale upon repeated oxide cracking requires easily accessible chromium in the alloy, mainly conveyed along alloy grain boundaries. This access becomes increasingly challenged with time not exclusively owing to depletion processes but also due to compound formation involving chromium in the alloy grain boundaries such as inherent carbon producing $Cr_{23}C_6$ and Cr_7C_3 as well as oxygen uptake along alloy grain boundaries. Here, possible oxidation-driven hydrogen uptake infers alloy vacancy pinning. Thus, access of Cr at the crack tip becomes increasingly impeded, while grain boundary oxidation is enhanced and correspondingly the risk for component failure.

The emerging mechanistic understanding elucidated in this work is

consistent with the following:

- Hydroxylated NiO grain boundaries are stable steady-state moieties in reactions of water with NiO(s) when water is the limiting reactant, e.g., owing to subsequent chromium oxidation.
- Transient nickel oxy-hydroxy-hydrides are formed, driven by the oxidation of chromium by the nickel oxy-hydroxide moieties.
- The biuld-up of nickel metal and nickel oxide heterostructures as transients disproportionate whereby hydrides H^- recombine with protons H^+
  - to produce H_2(g), i.e., the hydrogen evolution reaction, albeit being suppressed in vicinity of the oxide/alloy interface owing to the crack tip confinement;
  - to serve as a catalyst for the oxidation of chromium by nickel oxide to form metallic nickel particles, co-existing with nickel oxide and chromia in the vicinity of the crack tip;
  - to become absorbed in nickel metal particles as well as in the alloy in the vicinity of metal atom vacancies.

The competing processes, driven by the effective oxidation of chromium by water and controlled by the fates of hydrogen, provide a unified understanding of the complex oxide composition observed at the crack tip of nickel-base chromia formers. The fraction of hydrogen that becomes picked up by the alloy – but not in metallic nickel inclusions in the oxide or evolving as H_2 – is taken to be harmful at late stages when access to the chromium, decisive for the passivating oxide scale to form, becomes limited by its mobility. This situation is postponed in alloy 690 as compared to alloy 600.

CRediT authorship contribution statement

Ageo Meier de Andrade: Writing – review & editing, Writing – original draft, Visualization, Validation, Methodology, Investigation, Funding acquisition, Formal analysis, Data curation, Conceptualization. **Christine Geers:** Writing – review & editing, Writing – original draft, Conceptualization. **Jiaxin Chen:** Writing – review & editing, Writing – original draft, Funding acquisition, Conceptualization. **Itai Panas:** Writing – review & editing, Writing – original draft, Validation, Supervision, Resources, Project administration, Methodology, Funding acquisition, Formal analysis, Conceptualization.

Declaration of competing interest

The authors declare that they have no known competing financial interests or personal relationships that could have appeared to influence the work reported in this paper.

Data availability

All data generated from the calculations is available at the Swedish National Data repository (SND) and it can be accessed via the following link: https://doi.org/10.5878/406j-b839.

Acknowledgments

The authors aknowledge the funding provided by the Swedish Radiation Safety Authority [grant number 2021-7174] and the Swedish Research Council [grant numbers 2018-05973, 2022-06725, 2023-00209]. The computations were enabled by resources provided by the National Academic Infrastructure for Supercomputing in Sweden (NAISS) and the Swedish National Infrastructure for Computing (SNIC) provided by Chalmers e-Commons at Chalmers University of Technology.

References

[1] J.C. Scully, The theory of stress corrosion cracking in alloys, Anti-Corros. Method. Mater. 19 (1972) 5–10, https://doi.org/10.1108/eb006879.
[2] R.B. Rebak, Stress corrosion cracking (SCC) of nickel-based alloys, Stress Corros. Crack.: Theory Pract. (2011) 273–306, https://doi.org/10.1533/9780857093769.3.273.
[3] S. Lynch, Mechanistic and fractographic aspects of stress corrosion cracking, Corros. Rev. 30 (2012), https://doi.org/10.1515/corrrev-2012-0501.
[4] JoséR. Galvele, A stress corrosion cracking mechanism based on surface mobility, Corros. Sci. 27 (1987) 1–33, https://doi.org/10.1016/0010-938X(87)90117-X.
[5] V. Babic, V. Cantatore, C. Geers, I. Panas, J. Chen, On Water Induced Sensitisation of Ni (Fe,Cr) alloys towards stress corrosion cracking in LWR piping from 1st principles modelling, 2021. https://www.stralsakerhetsmyndigheten.se/publikationer/rapporter/sakerhet-vid-karnkraftverken/2021/202102/(accessed April 3, 2023).
[6] V.S. Raja, T. Shoji, Stress Corrosion Cracking : Theory and Practice, Woodhead Publishing, 2011.
[7] T.M. Angeliu, P.L. Andresen, F.P. Ford, Applying Slip-oxidation to the SCC of austenitic materials in BWR/PWR environments, (1998). (accessed September 5, 2023).
[8] M.M. Hall, Critique of the Ford–Andresen film rupture model for aqueous stress corrosion cracking, Corros. Sci. 51 (2009) 1103–1106, https://doi.org/10.1016/j.corsci.2009.02.022.
[9] T. Maeguchi, K. Sakima, K. Sato, K. Fujimoto, Y. Nagoshi, K. Tsutsumi, PWSCC Susceptibility of Alloy 690, 52 and 152. Minerals, Metals and Materials Series, Springer International Publishing, 2019, pp. 485–500, https://doi.org/10.1007/978-3-030-04639-2_30.
[10] G.S. Was, T.R. Allen, Corrosion issues in current and next-generation nuclear reactors, Struct. Alloy. Nucl. Energy Appl. (2019) 211–246, https://doi.org/10.1016/B978-0-12-397046-6.00006-X.
[11] M.A. Rodríguez, Corrosion control of nuclear steam generators under normal operation and plant-outage conditions: a review, Corros. Rev. 38 (2020) 195–230, https://doi.org/10.1515/corrrev-2020-0015.
[12] W. Kuang, G.S. Was, The effect of grain boundary structure on the intergranular degradation behavior of solution annealed alloy 690 in high temperature, hydrogenated water, Acta Mater. 182 (2020) 120–130, https://doi.org/10.1016/j.actamat.2019.10.041.
[13] W. Kuang, G.S. Was, A high-resolution characterisation of the initiation of stress corrosion crack in Alloy 690 in simulated pressurised water reactor primary water, Corros. Sci. 163 (2020) 108243, https://doi.org/10.1016/j.corsci.2019.108243.
[14] T. Moss, W. Kuang, G.S. Was, Stress corrosion crack initiation in Alloy 690 in high temperature water, Curr. Opin. Solid State Mater. Sci. 22 (2018) 16–25, https://doi.org/10.1016/j.cossms.2018.02.001.
[15] N. Hashimoto, S. Sakuraya, J. Tanimoto, S. Ohnuki, Effect of impurities on vacancy migration energy in Fe-based alloys, J. Nucl. Mater. 445 (2014) 224–226, https://doi.org/10.1016/j.jnucmat.2013.11.021.
[16] D. Tanguy, Y. Wang, D. Connétable, Stability of vacancy-hydrogen clusters in nickel from first-principles calculations, Acta Mater. 78 (2014) 135–143, https://doi.org/10.1016/j.actamat.2014.06.021.
[17] Y. Fukai, The metal-hydrogen system: basic bulk properties, Berlin, 2003, 2nd ed.
[18] K. Kawano-Miyata, Revisiting mechanisms for hydrogen-assisted fracturing of Ni-Fe-Cr alloys, Mater. Sci. Eng.: A 858 (2022) 144074, https://doi.org/10.1016/j.msea.2022.144074.
[19] J. Stjärnsäter, J. Chen, F. Lindberg, P. Ekström, P. Efsing, Effect of dissolved hydrogen on the crack growth rate and oxide film formation at the crack tip of alloy 600 exposed to simulated PWR primary water (2019) 423–437, https://doi.org/10.1007/978-3-030-04639-2_27.
[20] T. Terachi, N. Totsuka, T. Yamada, T. Nakagawa, H. Deguchi, M. Horiuchi, M. Oshitani, Influence of dissolved hydrogen on structure of oxide film on alloy 600 formed in primary water of pressurized water reactors, J. Nucl. Sci. Technol. 40 (2003) 509–516, https://doi.org/10.1080/18811248.2003.9715385.
[21] M. Lindgren, I. Panas, Oxygen vacancy formation, mobility, and hydrogen pick-up during oxidation of zirconium by water, Oxid. Met. 87 (2017) 355–365, https://doi.org/10.1007/s11085-016-9695-z.
[22] M. Lindgren, C. Geers, I. Panas, Possible origin and roles of nano-porosity in ZrO 2 scales for hydrogen pick-up in Zr alloys, J. Nucl. Mater. 492 (2017) 22–31, https://doi.org/10.1016/j.jnucmat.2017.05.017.
[23] D. Delafosse, T. Magnin, Hydrogen induced plasticity in stress corrosion cracking of engineering systems, Eng. Fract. Mech. 68 (2001) 693–729, https://doi.org/10.1016/S0013-7944(00)00121-1.
[24] Y. Yao, X. Pang, K. Gao, Investigation on hydrogen induced cracking behaviors of Ni-base alloy, Int. J. Hydrogen Energy 36 (2011) 5729–5738, https://doi.org/10.1016/j.ijhydene.2011.01.123.

[25] M. Uhlemann, B.G. Pound, Diffusivity, solubility and trapping behavior of hydrogen in alloys 600, 690tt and 800, Corros. Sci. 40 (1998) 645–662, https://doi.org/10.1016/S0010-938X(97)00167-4.

[26] J.-D. Hong, J. Lee, C. Jang, T.S. Kim, Low cycle fatigue behavior of alloy 690 in simulated PWR water—effects of dynamic strain aging and hydrogen, Mater. Sci. Eng.: A 611 (2014) 37–44, https://doi.org/10.1016/j.msea.2014.05.069.

[27] B. Ghule, C. Sundaresan, D. Vijayshankar, V.S. Raja, Oxidation behaviour of Ni-base superalloys in supercritical water: a review, J. Indian Inst. Sci. 102 (2022) 351–389, https://doi.org/10.1007/s41745-022-00289-x.

[28] M. Sennour, L. Marchetti, F. Martin, S. Perrin, R. Molins, M. Pijolat, A detailed TEM and SEM study of Ni-base alloys oxide scales formed in primary conditions of pressurised water reactor, J. Nucl. Mater. 402 (2010) 147–156, https://doi.org/10.1016/j.jnucmat.2010.05.010.

[29] L. Marchetti, F. Miserque, S. Perrin, M. Pijolat, XPS study of Ni-base alloys oxide films formed in primary conditions of pressurised water reactor, Surf. Interface Anal. 47 (2015) 632–642, https://doi.org/10.1002/SIA.5757.

[30] L. Marchetti, S. Perrin, Y. Wouters, F. Martin, M. Pijolat, Photoelectrochemical study of nickel base alloys oxide films formed at high temperature and high pressure water, Electrochim. Acta 55 (2010) 5384–5392, https://doi.org/10.1016/j.electacta.2010.04.063.

[31] J. Chen, A. Nurrochman, J.-D. Hong, T.S. Kim, C. Jang, Y. Yi, Comparison of oxide layers formed on the low-cycle fatigue crack surfaces of Alloy 690 and 316 SS tested in a simulated PWR environment, Nucl. Eng. Technol. 51 (2019) 479–489, https://doi.org/10.1016/j.net.2018.10.007.

[32] L. Marchetti, S. Perrin, F. Jambon, M. Pijolat, Corrosion of nickel-base alloys in primary medium of pressurised water reactors: new insights on the oxide growth mechanisms and kinetic modelling, Corros. Sci. 102 (2016) 24–35, https://doi.org/10.1016/j.corsci.2015.09.001.

[33] S.M. Bruemmer, L. Thomas, Insights into stress corrosion cracking mechanisms from high-resolution measurements of Crack-tip structures and compositions, MRS Proc. 1264 (2010), https://doi.org/10.1557/PROC-1264-BB01-09, 1264-BB01-09.

[34] S.S. Raiman, G.S. Was, Accelerated corrosion and oxide dissolution in 316L stainless steel irradiated in situ in high temperature water, J. Nucl. Mater. 493 (2017) 207–218, https://doi.org/10.1016/j.jnucmat.2017.05.043.

[35] W. Kuang, M. Song, G.S. Was, Insights into the stress corrosion cracking of solution annealed alloy 690 in simulated pressurised water reactor primary water under dynamic straining, Acta Mater. 151 (2018) 321–333, https://doi.org/10.1016/j.actamat.2018.04.002.

[36] K. Chen, Z. Shen, A study on the surface and crack tip oxidation of alloy 600 through high-resolution characterisation, Corros. Sci. 169 (2020) 108616, https://doi.org/10.1016/j.corsci.2020.108616.

[37] S. Voyshnis, A. Seyeux, S. Zanna, B. Martin-Cabanas, T. Couvant, P. Marcus, Oxide layer growth on nickel-base alloy surfaces in high temperature water and in O2 studied by ToF-SIMS with isotopic tracers, Corros. Sci. 145 (2018) 212–219, https://doi.org/10.1016/j.corsci.2018.10.009.

[38] W. Kuang, X. Wu, E.-H. Han, J. Rao, The mechanism of oxide film formation on Alloy 690 in oxygenated high temperature water, Corros. Sci. 53 (2011) 3853–3860, https://doi.org/10.1016/j.corsci.2011.07.038.

[39] J.-H. Liu, R. Mendonça, R.-W. Bosch, M.J. Konstantinović, Characterisation of oxide films formed on alloy 182 in simulated PWR primary water, J. Nucl. Mater. 393 (2009) 242–248, https://doi.org/10.1016/j.jnucmat.2009.06.012.

[40] Y. Wang, D. Connétable, D. Tanguy, Hydrogen influence on diffusion in nickel from first-principles calculations, Phys. Rev. B 91 (2015) 094106, https://doi.org/10.1103/PhysRevB.91.094106.

[41] I. Panas, J.-E. Svensson, H. Asteman, T.J.R. Johnson, L.-G. Johansson, Chromic acid evaporation upon exposure of Cr2O3(s) to H2O(g) and O2(g) – mechanism from first principles, Chem. Phys. Lett. 383 (2004) 549–554, https://doi.org/10.1016/j.cplett.2003.11.079.

[42] B. Pujilaksono, T. Jonsson, M. Halvarsson, I. Panas, J.-E. Svensson, L.-G. Johansson, Paralinear oxidation of chromium in O2 + H2O environment at 600–700°C, Oxid. Met. 70 (2008) 163–188, https://doi.org/10.1007/s11085-008-9114-1.

[43] M. Lindgren, G. Sundell, I. Panas, L. Hallstadius, M. Thuvander, H.-O. Andrén, Toward a comprehensive mechanistic understanding of hydrogen uptake in zirconium alloys by combining atom probe analysis with electronic structure calculations. Zirconium in the Nuclear Industry: 17th Volume, ASTM International, 2015, pp. 515–539, https://doi.org/10.1520/STP154320120164, 100 Barr Harbor Drive, PO Box C700, West Conshohocken, PA 19428-2959.

[44] T. Boll, V. Babic, I. Panas, O. Bäcke, K. Stiller, On aliovalent cations control of α-alumina growth on doped and undoped NiAl, Acta Mater. 210 (2021) 116809, https://doi.org/10.1016/j.actamat.2021.116809.

[45] V. Babic, C. Geers, I. Panas, Reactive element effects in high-temperature alloys disentangled, Oxid. Met. 93 (2020) 229–245, https://doi.org/10.1007/s11085-019-09946-6.

[46] N. Mortazavi, C. Geers, M. Esmaily, V. Babic, M. Sattari, K. Lindgren, P. Malmberg, B. Jönsson, M. Halvarsson, J.E. Svensson, I. Panas, L.G. Johansson, Interplay of water and reactive elements in oxidation of alumina-forming alloys, Nat. Mater. 17 (2018) 610–617, https://doi.org/10.1038/s41563-018-0105-6.

[47] V. Babic, C. Geers, B. Jönsson, I. Panas, Fates of hydrogen during alumina growth below Yttria nodules in FeCrAl(RE) at low partial pressures of water, Electrocatalysis 8 (2017) 565–576, https://doi.org/10.1007/s12678-017-0368-8.

[48] V. Cantatore, M.A. Olivas Ogaz, J. Liske, T. Jonsson, J.-E. Svensson, L.-G. Johansson, I. Panas, Oxidation driven permeation of iron oxide scales by chloride from experiment guided first-principles modeling, J. Phys. Chem. C 123 (2019) 25957–25966, https://doi.org/10.1021/acs.jpcc.9b06497.

[49] V. Cantatore, C. Geers, J. Chen, I. Panas, Insights into the zinc effect on radio-cobalt deposition on stainless steel piping surfaces under BWR conditions from experiment guided 1st principles modelling, J. Nucl. Mater. 540 (2020) 152361, https://doi.org/10.1016/j.jnucmat.2020.152361.

[50] W. Kohn, L.J. Sham, Self-consistent equations including exchange and correlation effects, Phys. Rev. 140 (1965) A1133–A1138.

[51] P. Hohenberg, W. Kohn, Inhomogeneous electron gas, Phys. Rev. 136 (1964) B864–B871.

[52] M.C. Payne, M.P. Teter, D.C. Allan, T.A. Arias, J.D. Joannopoulos, Iterative minimisation techniques for ab initio total-energy calculations - molecular-dynamics and conjugate gradients, Rev. Mod. Phys. 64 (1992) 1045–1097.

[53] S.J. Clark, M.D. Segall, C.J. Pickard, P.J. Hasnip, M.I.J. Probert, K. Refson, M. C. Payne, First principles methods using CASTEP, Zeitschrift Fur Kristallographie 220 (2005) 567–570, https://doi.org/10.1524/zkri.220.5.567.65075.

[54] J.P. Perdew, K. Burke, M. Ernzerhof, Generalised gradient approximation made simple, Phys. Rev. Lett. 77 (1996) 3865–3868, https://doi.org/10.1103/PhysRevLett.77.3865.

[55] J.P. Perdew, K. Burke, M. Ernzerhof, Erratum: generalised gradient approximation made simple (Physical Review Letters (1996) 77 (3865)), Phys. Rev. Lett. 78 (1997) 1396, https://doi.org/10.1103/PhysRevLett.78.1396.

[56] D.R. Hamann, M. Schlüter, C. Chiang, Norm-conserving pseudopotentials, Phys. Rev. Lett. 43 (1979) 1494, https://doi.org/10.1103/PhysRevLett.43.1494.

[57] H.J. Monkhorst, J.D. Pack, Special points for Brillouin-zone integrations, Phys. Rev. B 13 (1976) 5188–5192.

[58] J.D. Pack, H.J. Monkhorst, special points for Brillouin-zone integrations"-a reply, Phys. Rev. B 16 (1977) 1748–1749, https://doi.org/10.1103/PhysRevB.16.1748.

[59] R.H. Byrd, J. Nocedal, R.B. Schnabel, Representations of quasi-Newton matrices and their use in limited memory methods, Math. Prog. 63 (1994) 129–156.

[60] B.G. Pfrommer, M. Cote, S.G. Louie, M.L. Cohen, Relaxation of crystals with the quasi-Newton method, J. Comput. Phys. 131 (1997) 233–240.

[61] D. Zagorac, H. Müller, S. Ruehl, J. Zagorac, S. Rehme, Recent developments in the Inorganic Crystal Structure Database: theoretical crystal structure data and related features, J. Appl. Crystallogr. 52 (2019) 918–925, https://doi.org/10.1107/S160057671900997X.

[62] E.N. Maslen, V.A. Streltsov, N.R. Streltsova, N. Ishizawa, Synchrotron X-ray study of the electron density in α-Fe_2O_3, Acta Crystallogr. B. 50 (1994) 435–441, https://doi.org/10.1107/S0108768194002284.

[63] M.E. Fleet, The structure of magnetite, Acta Crystallogr. B. 37 (1981) 917–920, https://doi.org/10.1107/S0567740881004597.

[64] S. Sasaki, K. Fujino, Y. Takéuchi, X-ray determination of electron-density distributions in oxides, MgO, MnO, CoO, and NiO, and atomic scattering factors of their constituent atoms, Proc. Japn. Acad., Ser. B 55 (1979) 43–48, https://doi.org/10.2183/pjab.55.43.

[65] R.S. McEwen, Crystallographic studies on nickel hydroxide and the higher nickel oxides, J. Phys. Chem. 75 (1971) 1782–1789, https://doi.org/10.1021/j100681a004.

[66] E.R. Jette, F. Foote, Precision determination of lattice constants, J. Chem. Phys. 3 (1935) 605–616, https://doi.org/10.1063/1.1749562.

[67] H. Sawada, Residual electron density study of chromium sesquioxide by crystal structure and scattering factor refinement, Mater. Res. Bull. 29 (1994) 239–245, https://doi.org/10.1016/0025-5408(94)90019-1.

[68] G. Ueno, S. Sato, Y. Kino, The low-temperature tetragonal phase of $NiCr_2O_4$, Acta Crystallogr. C 55 (1999) 1963–1966, https://doi.org/10.1107/S0108270199011713.

[69] F. Müller, O.J. Kleppa, Thermodynamics of formation of chromite spinels, J. Inorg. Nucl. Chem. 35 (1973) 2673–2678, https://doi.org/10.1016/0022-1902(73)80497-X.

[70] G. Bertali, F. Scenini, M.G. Burke, The effect of residual stress on the preferential intergranular oxidation of alloy 600, Corros. Sci. 111 (2016) 494–507, https://doi.org/10.1016/j.corsci.2016.05.022.

[71] J. Nychka, Surface oxide cracking associated with oxidation-induced grain boundary sliding in the underlying alloy, Acta Mater. 52 (2004) 1097–1105, https://doi.org/10.1016/j.actamat.2003.10.042.

[72] J. Xiao, N. Prud'homme, N. Li, V. Ji, Influence of humidity on high temperature oxidation of Inconel 600 alloy: oxide layers and residual stress study, Appl. Surf. Sci. 284 (2013) 446–452, https://doi.org/10.1016/j.apsusc.2013.07.117.

[73] V.Y. Kazimirov, M.B. Smirnov, L. Bourgeois, L. Guerlou-Demourgues, L. Servant, A. M. Balagurov, I. Natkaniec, N.R. Khasanova, E.V. Antipov, Atomic structure and lattice dynamics of Ni and Mg hydroxides, Solid State Ion 181 (2010) 1764–1770, https://doi.org/10.1016/j.ssi.2010.10.002.

[74] D.S. Hall, D.J. Lockwood, C. Bock, B.R. MacDougall, Nickel hydroxides and related materials: a review of their structures, synthesis and properties, Proc. R. Soc. A: Math. Phys. Eng. Sci. 471 (2015), https://doi.org/10.1098/RSPA.2014.0792.

[75] W. Dennstedt, W. Löser, Zur kenntnis der nickelhydroxid-elektrode—III. Thermogravimetrische untersuchungen an Nickel(II)-hydroxiden, Electrochim. Acta 16 (1971) 429–435, https://doi.org/10.1016/0013-4686(71)85015-6.

[76] F.P. Kober, On the structure of electrochemically active hydrated nickel-oxide electrodes. Power Sources, Elsevier, 1967, pp. 257–268, https://doi.org/10.1016/B978-0-08-012176-5.50023-2.

[77] T.M. Angeliu, G.S. Was, The effect of chromium, carbon, and yttrium on the oxidation of nickel-base alloys in high temperature water, J. Electrochem. Soc. 140 (1993) 1877–1883, https://doi.org/10.1149/1.2220732.

[78] J.B. Ferguson, H.F. Lopez, Oxidation products of INCONEL alloys 600 and 690 in pressurised water reactor environments and their role in intergranular stress corrosion cracking, Metallurg. Mater. Trans. A 2006 37 8 (37) (2006) 2471–2479, https://doi.org/10.1007/BF02586220.

[79] F. Jambon, L. Marchetti, F. Jomard, J. Chêne, Mechanism of hydrogen absorption during the exposure of alloy 600-like single-crystals to PWR primary simulated media, J. Nucl. Mater. 414 (2011) 386–392, https://doi.org/10.1016/j.jnucmat.2011.04.066.
[80] X. Zhong, E.-H. Han, X. Wu, Corrosion behavior of Alloy 690 in aerated supercritical water, Corros. Sci. 66 (2013) 369–379, https://doi.org/10.1016/j.corsci.2012.10.001.
[81] S. Zumdahl, Chemical Principles, 2009.
[82] C. Ebensperger, B. Meyer, First-principles study of the reconstruction and hydroxylation of the polar NiO(111) surface, Physica Status Solidi(b) 248 (2011) 2229–2241, https://doi.org/10.1002/pssb.201147104.
[83] A. Barbier, G. Renaud, A. Stierle, The NiO(111)-(1×1) surface, Surf. Sci. (1998) 757–760, https://doi.org/10.1016/S0039-6028(97)01020-0, 402–404.
[84] L. Liu, S. Wang, S. Liu, Q. Guo, J. Guo, Interaction of water with faceted NiO(1 1 1) surface tuned by films thickness, Surf. Sci. 667 (2018) 8–12, https://doi.org/10.1016/j.susc.2017.09.010.
[85] W. Zhao, M. Bajdich, S. Carey, A. Vojvodic, J.K. Nørskov, C.T. Campbell, Water Dissociative Adsorption on NiO(111): energetics and Structure of the Hydroxylated Surface, ACS Catal 6 (2016) 7377–7384, https://doi.org/10.1021/acscatal.6b01997.
[86] F. Jambon, L. Marchetti, F. Jomard, J. Chêne, Characterisation of oxygen and hydrogen migration through oxide scales formed on nickel-base alloys in PWR primary medium conditions, Solid State Ion 231 (2013) 69–73, https://doi.org/10.1016/j.ssi.2012.10.012.
[87] Q. Peng, J. Hou, K. Sakaguchi, Y. Takeda, T. Shoji, Effect of dissolved hydrogen on corrosion of Inconel Alloy 600 in high temperature hydrogenated water, Electrochim. Acta 56 (2011) 8375–8386, https://doi.org/10.1016/j.electacta.2011.07.032.
[88] O.A. El kebir, A. Szummer, Comparison of hydrogen embrittlement of stainless steels and nickel-base alloys, Int. J. Hydrogen Energy 27 (2002) 793–800, https://doi.org/10.1016/S0360-3199(01)00151-3.
[89] A. Machet, A. Galtayries, P. Marcus, P. Combrade, P. Jolivet, P. Scott, XPS study of oxides formed on nickel-base alloys in high-temperature and high-pressure water, Surf. Interface Anal. 34 (2002) 197–200, https://doi.org/10.1002/sia.1282.
[90] F. Ning, X. Wu, J. Tan, Crevice corrosion behavior of Alloy 690 in high-temperature water, J. Nucl. Mater. 515 (2019) 326–337, https://doi.org/10.1016/j.jnucmat.2018.12.050.
[91] M. Sennour, P. Laghoutaris, C. Guerre, R. Molins, Advanced TEM characterisation of stress corrosion cracking of Alloy 600 in pressurised water reactor primary water environment, J. Nucl. Mater. 393 (2009) 254–266, https://doi.org/10.1016/j.jnucmat.2009.06.014.
[92] L.E. Thomas, S.M. Bruemmer, High-Resolution Characterization of Intergranular attack and stress corrosion cracking of alloy 600 in high-temperature primary water, CORROSION 56 (2000) 572–587, https://doi.org/10.5006/1.3280561.
[93] Y.-S. Chen, H. Lu, J. Liang, A. Rosenthal, H. Liu, G. Sneddon, I. McCarroll, Z. Zhao, W. Li, A. Guo, J.M. Cairney, Observation of hydrogen trapping at dislocations, grain boundaries, and precipitates, Science 367 (1979) 171–175, https://doi.org/10.1126/science.aaz0122 (2020).
[94] Ch.A. Wert, Trapping of hydrogen in metals. Hydrogen in Met 2, Springer-Verlag (Top in Appl Phys v 29), 1978, pp. 305–330, https://doi.org/10.1007/3-540-08883-0_24.
[95] M. Lindgren, I. Panas, Confinement dependence of electro-catalysts for hydrogen evolution from water splitting, Beilstein. J. Nanotechnol. 5 (2014) 195–201, https://doi.org/10.3762/bjnano.5.21.